Available online at www.sciencedirect.com
SCIENCE DIRECT
Journal of Catalysis 228 (2004) 141–151
JOURNAL OF CATALYSIS
www.elsevier.com/locate/jcat

Structural investigations of functionalized mesoporous silica-supported palladium catalyst for Heck and Suzuki coupling reactions

Ken-ichi Shimizu [a,*,1], Soichi Koizumi [a], Tsuyoshi Hatamachi [b], Hisao Yoshida [c], Shinichi Komai [d], Tatsuya Kodama [b], Yoshie Kitayama [b]

[a] *Graduate School of Science and Technology, Niigata University, Ikarashi-2, Niigata 950-2181, Japan*
[b] *Department of Chemistry & Chemical Engineering, Faculty of Engineering, Niigata University, Ikarashi-2, Niigata 950-2181, Japan*
[c] *Division of Environmental Research, EcoTopia Science Institute, Nagoya University, Nagoya 464-8603, Japan*
[d] *Department of Applied Chemistry, School of Engineering, Nagoya University, Chikusa-ku, Nagoya 464-8603, Japan*

Received 7 July 2004; revised 27 August 2004; accepted 3 September 2004

Available online 28 September 2004

Abstract

FSM-16 mesoporous silica-supported mercaptopropylsiloxane Pd(II) complex, Pd-SH-FSM, has been shown to act as an active, stabile, and recyclable heterogeneous catalyst for the Heck reaction of 4-bromoacetophenone with ethyl acrylate and for the Suzuki reaction of 4-bromoanisole with phenylboronic acid. The structure of the Pd species in Pd-SH-FSM before and after the reaction was well characterized by a combination of XRD, TEM, UV–vis, Pd *K*-edge XANES/EXAFS, and Pd L_{III}-edge XANES, and the results were compared with those of a amorphous silica-supported mercaptopropylsiloxane Pd(II) complex (Pd-SH–SiO_2), unmodified FSM-16-supported $Pd(OAc)_2$ (Pd-FSM), and previously reported heterogeneous catalysts (Pd zeolite and Pd/C). The aggregation behavior of Pd species during the reaction greatly depends on the support. On Pd-SH-FSM after Heck and Suzuki reactions, Pd(II) species coordinated to the sulfur ligands were the main Pd species together with small Pd clusters as minor species, and the catalyst was reused without marked loss in the activity. On Pd-SH–SiO_2, relatively large numbers of the Pd(II) species were converted to Pd clusters after the Suzuki reaction. On ligandless Pd-FSM, most of the Pd was aggregated to form Pd metal particles. The activity order of the recycled catalysts (Pd-SH-FSM > Pd-SH–SiO_2 > Pd-FSM) indicates that the Pd(II) complexes on the sulfur ligands and possibly the small Pd clusters are more active than Pd metal particles. It is concluded that the sulfur ligands in the size-restricted mesopore are effective for preventing the aggregation of coordinated Pd complexes, and this results in high durability and recycling characteristic of the Pd-SH-FSM. The deactivation of the Pd complex via Pd aggregation was significant for the conventional Pd catalysts; $[Pd(NH_3)_4]^{2+}$ complexes in Pd zeolite and PdO nanoclusters on Pd/C were changed to less reactive metal particles or clusters after Heck and Suzuki reactions.

Keywords: Heck reaction; Suzuki reaction; Palladium; Mesoporous silica; XAFS

1. Introduction

The olefination of aryl halides (Heck reaction) [1,2] and the coupling reaction of aryl halides with arylboronic acids (Suzuki reaction) [3,4] are well-established catalytic C–C coupling reactions. These reactions are generally catalyzed by soluble Pd complexes with phosphine ligands. However, homogeneous catalysts are generally connected with the problem of separation and wasted inorganics. In addition, the phosphine ligands and Pd precursors are usually difficult to handle because of their air-sensitive nature and are too difficult to reuse after the reaction. The stability of the Pd catalyst is also important for large-scale industrial application of the coupling reactions. It is generally assumed that the deactivation of the Pd complex occurs via aggregation

* Corresponding author. Fax: +81 52 789 3193.
E-mail address: kshimizu@apchem.nagoya-u.ac.jp (K. Shimizu).
[1] Present address: Department of Applied Chemistry, Graduate School of Engineering, Nagoya University, Chikusa-ku, Nagoya 464-8603, Japan.

0021-9517/$ – see front matter
doi:10.1016/j.jcat.2004.09.005

of palladium intermediates to clusters and further to inactive large metallic particles (Pd black). To overcome these problems, it is highly desirable to develop phosphine-free heterogeneous catalysts having a high stability and recyclability.

Although many supported Pd catalysts were reported to be effective for Heck [5–20] and Suzuki reactions [19–26], very few catalysts were shown to have both high stability of Pd species and successful recyclability. A typical strategy for obtaining phosphine-free solid catalysts is to immobilize Pd complexes or Pd nanoparticles on the supports, such as mesoporous silica [14], zeolites [15,16], and activated carbon [17,18]. Ying and co-workers reported that mesoporous silica-supported Pd nanoparticles showed good yield for the Heck reaction of aryl bromides, but recycling of this catalyst was hampered by significant Pd metal agglomeration [14]. Pd-exchanged zeolites were reported as more active Heck catalysts [15]. However, detailed TEM studies by Dams et al. evidenced Pd agglomeration and structural damage to the support after use in catalysis [16]. Köhler et al. tested a variety of Pd/C catalysts for the Heck reaction and showed that Pd/C with a high Pd dispersion and low degree of reduction was effective [18]. However, the average Pd crystallite size significantly increased after the reaction as a result of the dissolution and reprecipitation of Pd during the reaction, and the activity of the recycled catalyst was considerably low [18]. On the other hand, it was reported that colloidal Pd particles prepared from precipitation of simple Pd(II) salts in the presence of a protective shell ($R_4N + Br^-$ or polar polymers) catalyzed Heck [26] and Suzuki [27,28] reactions. However, such sols are not stable possibly because the protecting shell is stripped under the reaction conditions, which lead to the formation of inactive Pd black [2,27,28]. The Pd complex coordinated to the ligand-modified support is an another type of the heterogeneous catalysts. P-, N-, or S-containing groups linked to the surface of polymer [6–8] or silica [10–13,21–24] are believed to stabilize reactive Pd(II) or Pd(0) complexes. Among these studies, the Pd complex in diimine-modified mesoporous silica was shown to be a highly stable and reusable heterogeneous catalyst for the Suzuki reaction [22], though it was not shown that mesoporous supports offer advantages over amorphous silica. For this type of catalyst, it is suspected that Pd complexes are converted to Pd clusters or particles during the reaction. However, very few structural studies have focused on this aspect, and hence the structure of the active Pd species is still speculatively understood. Hence, we considered that detailed structural characterizations of the Pd catalyst after the reaction and a systematic study of the structure–activity relationship of the reused catalysts are indispensable for clarifying the nature of the active Pd species.

From the above examples, the development of heterogeneous Pd catalysts that preserve high Pd dispersion during the coupling reactions is desirable. Based on the reports that sulfur-containing molecules such as thiols strongly coordinate to the cationic noble metal species [29] as well as metallic species such as Au and Pt nanoparticles [30,31], we hypothesized that SH groups in the mesopore can act as polydentate ligands to stabilize both Pd(II) complexes and metallic Pd species by a size restriction and an isolation of unstable Pd species. In this study, we show that the mesoporous silica (FSM-16)-supported mercaptopropylsiloxane palladium(II) complex, Pd-SH-FSM, is highly resistant to the metal agglomeration and acts as a durable and reusable catalyst for Heck and Suzuki reactions. A detailed structural analysis before and after the reaction is performed to reveal the structural changes during the reaction, and the results are discussed in terms of the effects of the sulfur ligands and the mesoporous support on the stability of the active Pd species. The structural aspect of Pd-SH-FSM is also compared with those of previously reported catalysts (Pd zeolite and Pd/C) to demonstrate the high stability of Pd-SH-FSM.

2. Experimental

2.1. Catalyst preparation and characterization

The reagents were obtained from commercial sources and were used without further purification. FSM-16 was prepared from kanemite ($NaHSi_2O_5{\cdot}3H_2O$) using $C_{16}H_{33}NMe_3Cl$ as a template, according to a method previously described [32]. Kanemite crystals (10 g) were synthesized by calcination of water glass ($SiO_2/Na_2O = 2.14$, Aichikeiso Industry Co. Ltd.) at 973 K for 6 h, followed by dispersion in 300 cm^3 distilled water with stirring for 3 h. The wet kanemite was dispersed in 100 cm^3 of a 0.1 mol dm^{-3} $C_{16}H_{33}NMe_3Cl$ aqueous solution and heated at 343 K for 3 h, adjusting the pH of the solution to 12–12.4 with NaOH solution, and further stirring at 343 K for 3 h, adjusting the pH of the solution to 8.3 with HCl. After filtration, the white precipitate was calcined at 973 K for 4 h to eliminate the surfactant. The SH groups were anchored on FSM-16 silica by the postmodification method. The FSM-16 sample (2.0 g) was dried at 393 K, and then 3-mercaptopropyltriethoxysilane (4 mmol) in dry toluene (20 mL) was introduced. The mixture was refluxed for 6 h, and the solid was filtered off, washed with toluene and acetone, and air-dried. FSM-16-supported mercaptopropylsiloxane palladium(II) complex, Pd-SH-FSM, was prepared by stirring the mercaptopropyl-functionalized FSM-16 (SH-FSM) with a solution of $Pd(OAc)_2$ in acetone at 298 K for 12 h. The filtered catalyst powders were washed by refluxing in ethanol, toluene, and then acetonitrile to remove any physisorbed Pd species [22], followed by filtering and drying in vacuo at 298 K. SH-fuctionalized amorphous silica (SH-SiO_2) was prepared by a sol–gel method. To a solution of ethanol (20 mL) with deionized water (15 mL), 47.8 mmol of tetraethylorthosilicate ($Si(OEt)_4$) and 3.55 mmol of 3-mercaptopropyltriethoxysilane were added and the mixture was stirred at 353 K for 2 h. The wet gel was filtered and washed with ethanol, followed by drying

in vacuo at 298 K. The amorphous silica-supported mercaptopropylsiloxane palladium(II) complex (Pd-SH–SiO_2) was prepared from SH-SiO_2 and $Pd(OAc)_2$ following the same procedure as that for Pd-SH-FSM. ICP and elemental analysis showed that compositions of these samples are close to each other: Pd-SH-FSM (Pd = 0.40 mmol g^{-1}, S = 1.11 mmol g^{-1}, Pd/S ratio = 0.36), Pd-SH-SiO_2 (Pd = 0.34 mmol g^{-1}, S = 0.95 mmol g^{-1}, Pd/S ratio = 0.36).

For comparison, the unmodified FSM-16-supported $Pd(OAc)_2$, called Pd-FSM, was prepared by impregnating the FSM-16 with a solution of $Pd(OAc)_2$ in acetone at 298 K for 12 h, followed by drying in vacuo at 298 K. The $[Pd(NH_3)_4]^{2+}$-exchanged NaY zeolite (Pd-Y) was prepared by exchanging the NaY zeolite (JRC-Z-Y 5.6, SiO_2/Al_2O_3 = 5.6, surface area = 870 $m^2\,g^{-1}$) with an aqueous solution of $[Pd(NH_3)_4]Cl_2$ at 298 K for 48 h, followed by centrifuging and washing with water, and subsequently drying in vacuo at 298 K. 15 Pd/C (Pd content = 5 wt%, water content = 54.2 wt%) was purchased from Kawaken Fine Chemicals, Co., Ltd.

The BET surface area and pore-size distribution were obtained by measuring N_2 adsorption isotherms at 77 K by using a TriStar 3000 (Micromeritics). XRD patterns were taken by MX Labo (MAC Science) with Cu$K\alpha$ radiation (40 kV, 25 mA). Diffuse reflectance spectra of powder samples were obtained with a UV–vis spectrometer (Jasco; V-550) and were converted from reflection to absorbance by the Kubelka–Munk method. Transmission electron microscopy (TEM) was carried out on a JEOL JEM-2010 operating at 200 kV. Pd K-edge XAFS was conducted in transmission mode at BL-10B (Photon Factory in High Energy Accelerator Research Organization, Tsukuba, Japan) with a Si(311) channel-cut monochromator. Pd L_{III}-edge XANES spectra were obtained at the BL-9A station of the Photon Factory in transmission mode with a Si(111) double-crystal monochromator. High-energy X-rays from high-order reflections were removed by a pair of flat quartz mirrors coated with Rh/Ni that were aligned in parallel. The ionization chambers filled with N_2(30%)–He(70%) for I_0 (17 cm) and N_2(100%) for I (31 cm) were used. For Pd K and Pd L_{III} XAFS, the energy was defined by assigning the first inflection point of the Cu foil spectrum to 8980.3 eV. Normalization of XANES and EXAFS analyses were carried out as described elsewhere [33]. For the curve-fitting analysis of Pd–O, Pd–S, and Pd–Pd shells in the Pd K-edge EXAFS, parameters extracted from $Pd(OAc)_2$, $PdCl_2$, and Pd foil were used, respectively.

2.2. Catalytic test

To prepare the samples for the catalyst characterization after Suzuki and Heck reactions, the following reaction conditions were used. For the Suzuki reaction, 4-bromoanisole (5.0 mmol), phenylboronic acid (6.0 mmol), K_2CO_3 (7.5 mmol), benzonitrile (1 mmol, internal standard), and the catalyst (1 mol%) were stirred in DMF (5 mL) at 403 K under N_2. For Heck reaction, 4-bromoacetophenone (3.0 mmol), ethyl acrylate (4.5 mmol), KOAc (4.5 mmol), benzonitrile (1 mmol, internal standard), and the catalyst (1 mol%) were stirred in NMP (5 mL) at 403 K under N_2. For the kinetic experiments of Suzuki and Heck reactions, the following reaction conditions were used. For the Suzuki reaction, 4-bromoanisole (25 mmol), phenylboronic acid (30 mmol), K_2CO_3 (37 mmol), benzonitrile (5 mmol, internal standard), and the catalyst (0.013 mol%) were stirred in DMF (50 mL) at 403 K under N_2. For the Heck reaction, 4-bromoacetophenone (50 mmol), ethyl acrylate (75 mmol), KOAc (75 mmol), benzonitrile (10 mmol, internal standard), and the catalyst (0.0013 mol%) were stirred in NMP (50 mL) at 403 K under N_2. Samples were withdrawn periodically and analyzed by GC. The isolated products obtained by separate experiments were analyzed by ^{1}H NMR (JEOL NM-EXCALIBUR 270) to confirm the GC analysis.

3. Results and discussion

3.1. Structure of the as-prepared catalyst

The XRD pattern of Pd-SH-FSM showed a typical low-angle reflection (100) at d_{100} = 3.65 nm characteristic of FSM-16 [32], indicating that the long-range ordered structure of the support was preserved. For FSM-16, surface area (881 $m^2\,g^{-1}$), pore volume (1.32 $cm^3\,g^{-1}$), and pore diameters (around 2.6 nm) were as expected for mesoporous materials. These values were reduced after the introduction of the mercaptopropylsiloxane palladium(II) complex: surface area (724 $m^2\,g^{-1}$), pore volume (0.84 $cm^3\,g^{-1}$), and pore diameters (around 2.3 nm) for Pd-SH-FSM. This suggests the presence of the complex in the channels of FSM-16.

To clarify the nature of the Pd species on the catalysts, UV–vis and XAFS analyses were performed. As shown in Fig. 1, UV–vis diffuse reflectance spectra of Pd-SH-FSM and Pd-SH–SiO_2 exhibit a broad band around 340–360 nm due to the d–d transition of Pd(II) complex. Its position is higher in energy than that of $Pd(OAc)_2$ in acetone (400 nm). Generally, the energy of the d–d transition peak increases with a decrease in the electronegativity of the bonding atom. Thus, the positive shifts in energy after an introduction of $Pd(OAc)_2$ into SH-FSM and SH-SiO_2 suggest the partial substitution of the OAc^- ligand by the sulfur ligand.

X-ray absorption near-edge structures (XANES) around the Pd K edge are shown in Fig. 2. In the spectrum of $Pd(OAc)_2$, a peak at 24370 eV is observed. The spectra of Pd-SH-FSM and Pd-SH–SiO_2, having a peak at 24372 eV, are very close to each other. Although their positions are close to that of $Pd(OAc)_2$, the peaks for Pd-SH-FSM and Pd-SH–SiO_2 are broader than that for $Pd(OAc)_2$. This indicates that the structure of Pd(II) complex on these catalysts is slightly different from that of $Pd(OAc)_2$, the starting material, possibly due to the interaction with SH groups. Fig. 3 shows the Fourier transforms of k^3-weighted EXAFS spec-

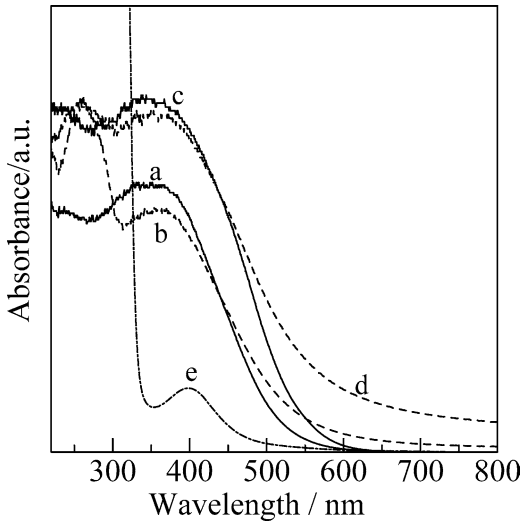

Fig. 1. UV–vis spectra of (a) Pd-SH-FSM, (b) Pd-SH-FSM after the Suzuki reaction, (c) Pd-SH–SiO_2, (d) Pd-SH–SiO_2 after the Suzuki reaction, and (e) 0.3 mM $Pd(OAc)_2$ in acetone.

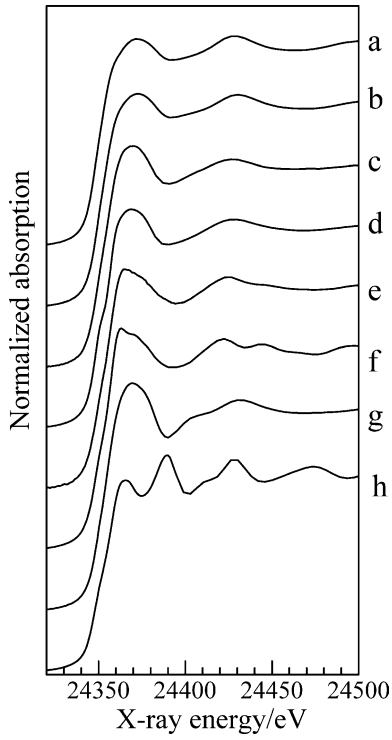

Fig. 2. Pd K-edge XANES spectra of the fresh catalysts and reference compounds: (a) Pd-SH-FSM, (b) Pd-SH–SiO_2, (c) Pd-FSM, (d) Pd-Y, (e) Pd/C, (f) PdO, (g) $Pd(OAc)_2$, (h) Pd foil.

tra at the Pd K edge for the catalysts and reference compounds ($Pd(OAc)_2$, $PdCl_2$, PdO, and Pd foil). A peak centered around 0.16 nm (phase-shift uncorrected), observed on the spectrum of $Pd(OAc)_2$, are assigned to the backscattering from the adjacent oxygen atoms. For Pd-FSM, a peak at 0.16 nm is observed, suggesting that a $Pd(OAc)_2$-like complex is supported on FSM-16. Note that $Pd(OAc)_2$ consists of the PdO_4 square plane with a Pd–O distance of 0.199 nm

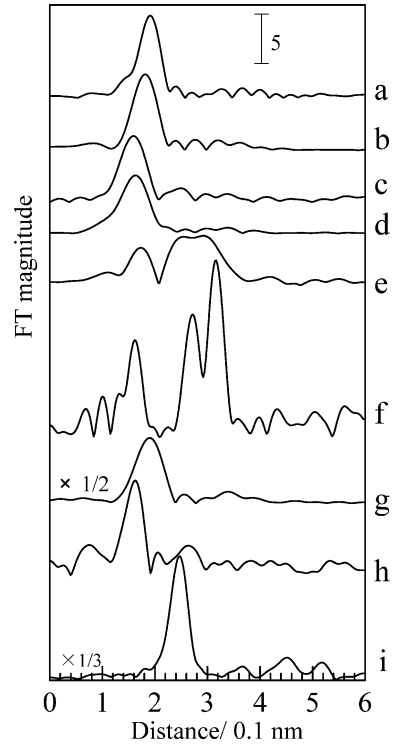

Fig. 3. Fourier transforms of k^3-weighted EXAFS spectra of the fresh catalysts and reference compounds: (a) Pd-SH-FSM, (b) Pd-SH–SiO_2, (c) Pd-FSM, (d) Pd-Y, (e) Pd/C, (f) PdO, (g) $PdCl_2$, (h) $Pd(OAc)_2$, (i) Pd foil.

[34], while $PdCl_2$ consists of the $PdCl_4$ square plane with Pd–Cl distance of 0.231 nm [35]. The peak position for the Pd–Cl shell of $PdCl_2$ (0.19 nm) is higher than that for the Pd–O shell of $Pd(OAc)_2$, which reflects the longer distance of the former bond. For Pd-SH-FSM, the position of the first shell (0.19 nm) is close to that for the Pd–Cl shell of $PdCl_2$. For Pd-SH–SiO_2, the position of the first shell (0.18 nm) is also higher than that for Pd–O shell of $Pd(OAc)_2$. These results indicate the coordination of a larger atom at a larger distance than Pd–O bond length, implying the presence of S atoms at the first coordination sphere of Pd atoms. At higher distances, the spectra of Pd-SH-FSM, Pd-SH–SiO_2, and Pd-FSM are featureless, indicating a lack of long-range order. Table 2 shows the structural parameters determined by the curve-fitting analysis. For Pd-SH-FSM and Pd-SH–SiO_2 samples, the analysis was unsuccessful with a Pd–O shell, and the optimum fitting result gives around 2.3–2.6 Pd–S bonds of 0.230 nm and around 0.3–0.6 Pd–O bonds of 0.200 nm. This indicates that the Pd(II) complex is coordinated to at least two sulfur ligands on the supports. For $Pd(OAc)_2$-impregnated FSM-16 (Pd-FSM), the optimum fitting result gives 4.5 Pd–O bonds of 0.200 nm, indicating that $Pd(OAc)_2$ is supported on FSM-16 without changing its local structure. This model is supported by the XANES result (Fig. 2); the spectral feature and edge position for Pd-FSM are very close to those for $Pd(OAc)_2$.

Pd L_{III}-edge XANES spectra of various Pd compounds and Pd-SH-FSM are shown in Fig. 4. All the spectra for Pd(II) compounds exhibited a large white line peak centered

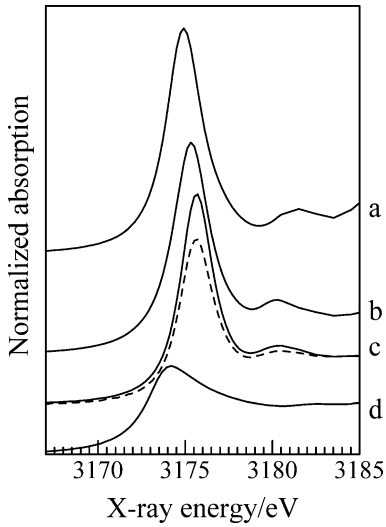

Fig. 4. Pd L_{III}-edge XANES spectra of (a) $PdCl_2$, (b) $Pd(OAc)_2$, (c) Pd-SH-FSM, and (d) Pd black. A dotted line denotes the spectrum for the Pd-SH-FSM after Heck reaction.

around 3175–3176 eV. This peak can be assigned to the electronic transition from the Pd $2p_{3/2}$ to the unoccupied $4d$ states [36]. According to the earlier report on the Pd L_{III}-edge XANES of Pd(II) compounds, the energy position of the white line increases with a decrease in the electronegativity of the bonding atom [36]. The position of the white line peak for Pd-SH-FSM is higher than that of $Pd(OAc)_2$. This result suggests the coordination of the less electronegative atom, i.e., sulfur, to Pd(II), which is consistent with the UV–vis and Pd K-edge XAFS results. In summary, it is shown that Pd(II) species coordinated to at least two sulfur ligands are present in the Pd-SH-FSM and Pd-SH–SiO_2 catalysts.

As shown in Fig. 2, the spectral features of XANES for Pd/C are similar to those for PdO. The EXAFS spectrum of Pd/C showed a peak at 0.17 nm assignable to the adjacent oxygen atom, and its spectral features are close to that of PdO. TEM image of Pd/C showed that the particle size was around 2–5 nm (not shown). From these results, it is shown that the highly dispersed PdO nanoclusters are the main Pd species on Pd/C used in this study. UV–vis spectrum of Pd-Y showed a band at 300 nm due to the d–d transition of $[Pd(NH_3)_4]^{2+}$ complexes in NaY zeolite [37], which indicates that $[Pd(NH_3)_4]^{2+}$ complexes are exchanged in NaY zeolite.

3.2. Structural change of the catalyst during the Suzuki reaction

To investigate the structure of the catalysts after the Suzuki reaction, the coupling reaction of 4-bromoanisole and phenylboronic acid was first carried out with the catalysts listed in Table 1 under the same conditions (Pd = 1 mol%). Each catalyst showed a good to high yield of coupling products (73–92%). After each experiment, the amount of Pd in solution was determined by ICP after removal of the solid catalyst by filtration. The proportion of the Pd leached in solution strongly depended on the type of the catalyst and changed in the following order: Pd-SH-FSM (0.05%) < Pd-SH–SiO_2 (0.06%) < Pd/C (0.09%) < Pd-FSM (2.23%) < Pd-Y (6.03%). The filtered catalyst was washed by acetone and water and dried in vacuo at 298 K, and the obtained catalyst powder was characterized in detail as shown below. The color of Pd-FSM and Pd-Y catalysts changed to gray after the reaction, suggesting the formation of the Pd particles. Pd-SH-FSM did not change its color (yellow). In contrast, Pd-SH–SiO_2 changed its color from yellow to brown. This color change is reflected in UV–vis spectrum of Pd-SH–SiO_2 after the reaction (Fig. 1d). For both samples the band at 350 nm remained unchanged, indicating that the Pd(II) complex coordinated to the sulfur ligand is present on the used catalysts. For the used Pd-SH–SiO_2 sample, the absorption in the visible region due to the band structure of metal nanoparticles [26,28,38] is observed, which suggests the presence of Pd nanoparticles. This feature is not significantly observed for Pd-SH-FSM.

The XRD patterns of the catalysts after the Suzuki reaction are shown in Fig. 5. In the XRD patterns of Pd-FSM, Pd-Y, and Pd/C, a small line around $2\theta = 40°$ due to Pd metal (plane 111) was observed. No lines due to Pd metal were observed in the XRD pattern of Pd-SH-FSM. TEM image showed that roughly spherical 2- to 8-nm-diameter Pd nanoparticles were formed in the used sample of Pd-SH–SiO_2 (Fig. 6b). As for the used Pd-FSM, small Pd metal particles (10–20 nm) were observed by TEM (Fig. 6c). In

Table 1
Physical characteristics of catalysts and results of Heck and Suzuki coupling reactions

Catalysts	Pd (wt%)	Surface area ($m^2\ g^{-1}$)	Color	Suzuki reaction[a]			Heck reaction[b]		
				Yield (%)	Pd leaching (%)	Color	Yield (%)	Pd leaching (%)	Color
Pd-SH-FSM	3.4	724	Yellow	79	0.05	Yellow	92	0.01	Yellow
Pd–SiO_2-SH	3.6	689	Yellow	73	0.06	Brown	84	0.23	Brown
Pd-FSM	1.2	648	Brown	77	2.23	Gray	96	0.39	Gray
Pd-Y	2	(870)	White	83	6.03	Gray	95	4.08	Gray
Pd/C	5	443	Black	86	0.09	Black	87	0.15	Black

[a] Conditions: 4-bromoanisole (5.0 mmol), phenylboronic acid (6.0 mmol), K_2CO_3 (7.5 mmol), benzonitrile (1 mmol, internal standard, and the catalyst (1 mol%) were stirred in DMF (5 mL) at 403 K under N_2.

[b] Conditions: 4-bromoacetophenone (3.0 mmol), ethyl acrylate (4.5 mmol), KOAc (4.5 mmol), benzonitrile (1 mmol, internal standard), and the catalyst (1 mol%) were stirred in NMP (5 mL) at 403 K under N_2.

Table 2
Curve-fitting analysis of Pd K-edge EXAFS for as-prepared samples

Catalysts	Shell	CN	R (Å)	σ^2 (Å^2)	ΔE_0 (eV)
Pd-SH-FSM	O	0.6	2.00	0.0033	4
	S	2.6	2.30	−0.0002	4
Pd-SH–SiO_2	O	0.3	2.00	−0.0075	4
	S	2.3	2.27	−0.0008	4
Pd-FSM	O	4.5	2.02	0.0013	1

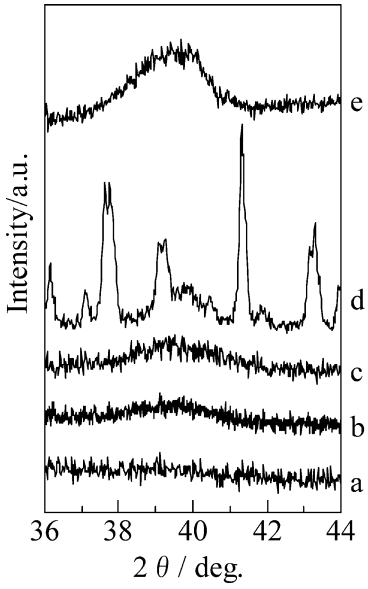

Fig. 5. XRD patterns of the catalysts after the Suzuki reaction: (a) Pd-SH-FSM, (b) Pd-SH–SiO_2, (c) Pd-FSM, (d) Pd-Y, (e) Pd/C.

contrast, such Pd nanoparticles were not clearly seen in the TEM image of Pd-SH-FSM (Fig. 6a). In the case of Pd-Y after the Suzuki reaction, relatively large Pd metal particles (20–60 nm) were mainly observed (Fig. 6d).

UV–vis, XRD, and TEM analyses do not give quantitative information from all Pd species in the samples. Whereas, XAFS spectroscopy (XANES and EXAFS) potentially provides an average structural information of all the Pd species in the sample. As shown in Fig. 7A, the Pd K-edge XANES of the Pd-SH-FSM after the reaction is almost the same as that of the fresh sample. In the EXAFS spectrum of the Pd-SH-FSM and Pd-SH–SiO_2 after the reaction (Fig. 7B), a peak due to the coordinating ligand (0.19 nm) and a peak due to the adjacent Pd atom (0.25 nm) are observed. The curve-fitting results (Table 3) show that the structural parameters for the first shell of Pd-SH-FSM and Pd-SH–SiO_2 have not significantly changed after the reaction, which indicate the presence of the Pd(II) coordinated to at least two sulfur ligands even after the reaction. The peak due to Pd–Pd is more intense for Pd-SH–SiO_2, resulting in the higher coordination number (3.6) than that for Pd-SH-FSM (0.5). The larger Pd–Pd coordination number of Pd-SH–SiO_2 indicates the presence of a larger number of Pd metal particles or the larger Pd metal particles on this sample, which is consistent with the TEM result.

Table 3
Curve-fitting analysis of Pd K-edge EXAFS for the catalysts after the Suzuki reaction

Catalysts	Shell	CN	R (Å)	σ^2 (Å^2)	ΔE_0 (eV)
Pd-SH-FSM	O	0.7	2.00	0.0087	4
	S	2.7	2.30	0.0018	4
	Pd	0.5	2.89	0.0189	0
Pd-SH–SiO_2	O	0.6	2.00	0.0169	4
	S	2.5	2.30	0.0014	4
	Pd	3.6	2.79	0.0042	3
Pd-FSM	Pd	11.1	2.77	0.0085	0
Pd-Y	Pd	10.1	2.80	0.0078	0
Pd/C	Pd	8.3	2.79	0.0036	−3

XANES spectra of Pd-FSM, Pd-Y, and Pd/C catalysts significantly changed after the reaction; their feature was very close to that of Pd foil. In EXAFS spectra of Pd-FSM, Pd-Y, and Pd/C after the reaction, peaks around 0.16–0.17 nm due to the coordinating ligands (Pd–O or Pd–N) completely disappeared, and intense peaks at 0.25 nm due to the adjacent Pd atoms in Pd metals appeared. This indicates that, during the reaction, $Pd(OAc)_2$-like complexes on unmodified FSM, $[Pd(NH_3)_4]^{2+}$ complexes exchanged in NaY zeolite and PdO nanoparticles on Pd/C were completely reduced and aggregated to form Pd particles. The coordination numbers of the Pd–Pd shell (Table 3) ranged from 8.3 to 11.1, and these values were smaller than that of Pd foil (12), which suggests that the Pd particles on these samples have a small particle size.

From these results, we have determined the catalyst structure after the Suzuki reaction as follows. On Pd-SH-FSM, Pd(II) complexes coordinated to at least two sulfur ligands were the main Pd species, together with Pd nanoclusters undetectable by TEM as minor species. Whereas, on ligandless Pd-FSM, Pd-Y, and Pd/C, most of the Pd(II) species (Pd(II) complexes or PdO nanoclusters) were aggregated during the reaction to form Pd metal particles. On Pd-SH–SiO_2, some part of the Pd(II) complexes coordinated to the sulfur ligand were converted to Pd clusters (2–8 nm) after the reaction.

3.3. Structural change of the catalyst during the Heck reaction

The Heck reaction of 4-bromoacetophenone and ethyl acrylate was carried out to obtain the used catalyst samples. As shown in Table 1, each catalyst showed a good to high yield of coupling products (84–96%) under this condition. After each experiment, the amount of Pd in solution was determined by ICP after removal of the solid catalyst by filtration. The proportion of the Pd leached in solution changed in the following order: Pd-SH-FSM (0.01%) < Pd/C (0.15%) < Pd-SH–SiO_2 (0.23%) < Pd-FSM (0.39%) < Pd-Y (4.08%). To compare the structural stability of each catalyst, the recovered catalyst powder was characterized as shown below. In the XRD patterns of Pd-SH-FSM and Pd-SH–SiO_2 after the reaction (not shown), no detectable lines due to metallic Pd were observed, whereas a

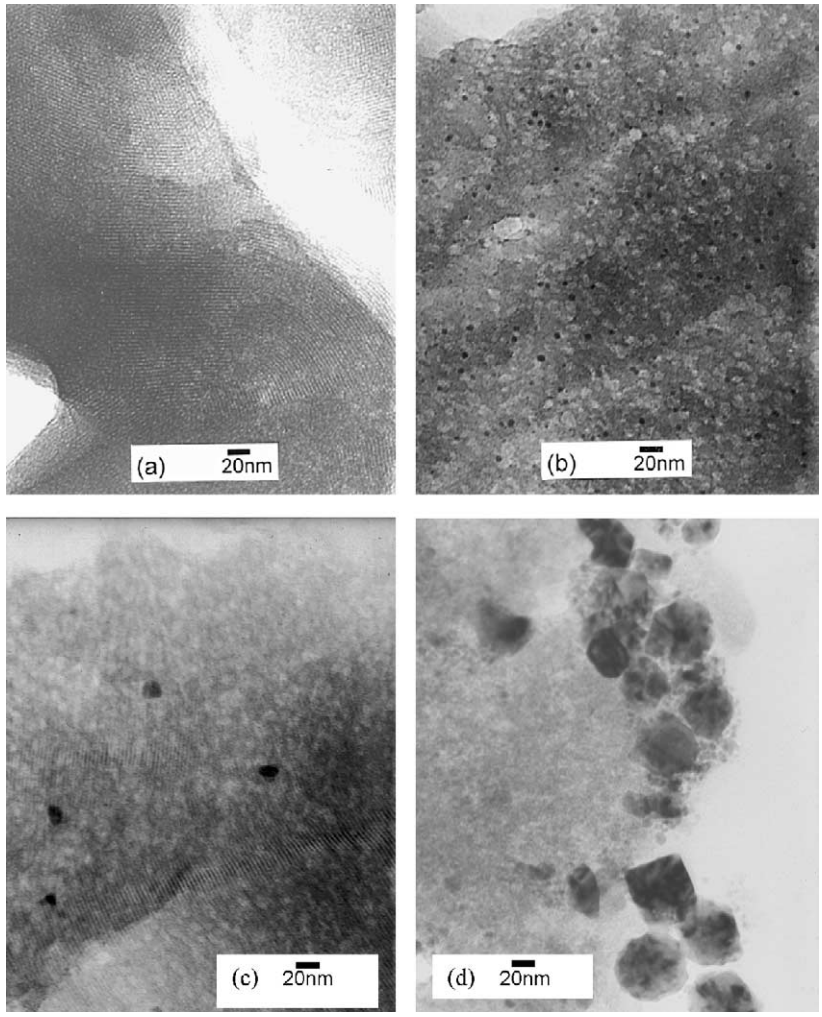

Fig. 6. TEM images of (a) Pd-SH-FSM, (b) Pd-SH–SiO_2, (c) Pd/FSM, and (d) Pd-Y after the Suzuki reaction.

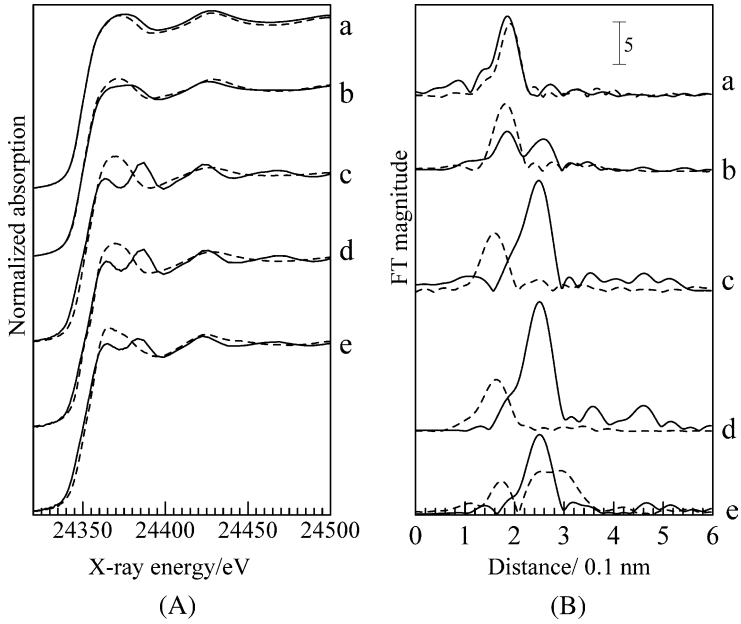

Fig. 7. (A) Pd K-edge XANES spectra and (B) Fourier transforms of k^3-weighted EXAFS spectra of the catalysts after the Suzuki reaction: (a) Pd-SH-FSM, (b) Pd-SH–SiO_2, (c) Pd-FSM, (d) Pd-Y, (e) Pd/C. Dotted lines denote the spectra for the fresh catalysts.

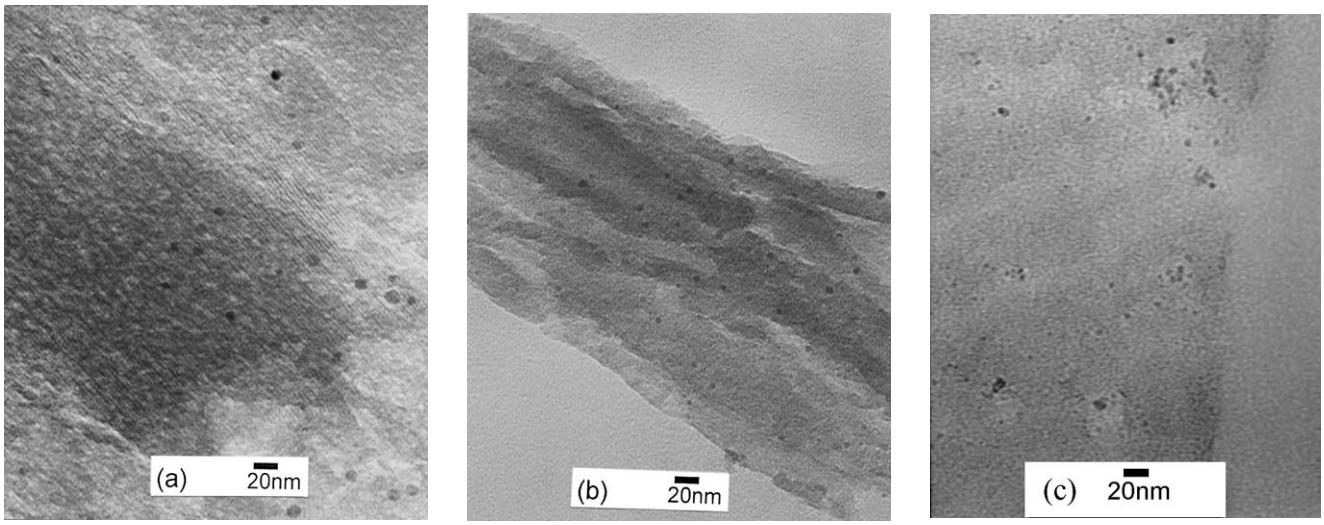

Fig. 8. TEM images of (a) Pd-SH-FSM, (b) Pd-SH–SiO_2, and (c) Pd/C after the Heck reaction.

Table 4
Curve-fitting analysis of Pd K-edge EXAFS for the catalysts after Heck reaction

Catalysts	Shell	CN	R (Å)	σ^2 (Å^2)	ΔE_0 (eV)
Pd-SH-FSM	O	0.5	2.00	0.0034	4
	S	2.8	2.29	0.0013	4
	Pd	0.5	2.75	0.0024	4
Pd-SH–SiO_2	O	0.6	2.00	0.0091	4
	S	2.5	2.30	0.0014	4
	Pd	1.4	2.82	0.0043	0
Pd-FSM	Pd	8.6	2.75	0.0010	−9
Pd-Y	Pd	9.7	2.76	0.0029	0
Pd/C	Pd	9.9	2.80	0.0066	0

very broad line due to metallic Pd ($2\theta = 40°$) was observed for Pd-Y, Pd-FSM, and Pd/C. UV–vis spectra of Pd-SH-FSM and Pd-SH–SiO_2 after the reaction (not shown) showed the band at 350 nm, indicating the presence of Pd(II) complexes. The TEM images of Pd-SH-FSM and Pd-SH–SiO_2 after the Heck reaction (Fig. 8) showed that 2- to 14-nm-diameter Pd nanoparticles were formed in both samples. XANES spectra and Fourier transforms of k^3-weighted EXAFS at the Pd K edge of recovered catalysts are shown in Figs. 9A and B, respectively. EXAFS spectra of Pd-SH-FSM and Pd-SH–SiO_2 after the reaction showed an intense peak at 0.19 nm mainly due to Pd–S bonds (Table 4) and a very small shoulder around 0.25–0.27 nm due to Pd–Pd bonds. The curve-fitting results of Pd-SH-FSM and Pd-SH–SiO_2 (Table 4) show 2.8 and 2.5 Pd–S bonds around 0.23 nm, 0.5 and 0.6 Pd–O bonds at 0.200 nm, and 0.5 and 1.4 Pd–Pd bonds at 0.275–0.282 nm, respectively. This result indicates the presence of the Pd(II) coordinated to at least two sulfur ligands as the main species and small Pd clusters, shown by TEM, as the minor species. The XANES spectrum of Pd-SH-FSM after the reaction is very close to that of fresh sample, indicating that most of the Pd exist as divalent species. In contrast, XANES spectra of Pd-FSM, Pd-Y, and Pd/C catalysts after the reaction were very close to that of Pd foil. EXAFS spectra of these samples exhibit intense peaks due to Pd–Pd bonds (0.25 nm). TEM images show that the Pd particle sizes on Pd/C (Fig. 8c), Pd-Y (not shown), and Pd-FSM (not shown) are 2–10, 20–60, and 8–30 nm, respectively. It is clear that Pd(II) precursors on the fresh catalysts, i.e., $Pd(OAc)_2$ on unmodified FSM, $[Pd(NH_3)_4]^{2+}$ in NaY zeolite, and highly dispersed PdO nanoclusters on Pd/C, were completely changed to metallic Pd particles (Pd-Y and Pd-FSM) or Pd metal nanoclusters (Pd/C). A Pd L_{III}-edge XANES spectrum of the Pd-SH-FSM after the Heck reaction is shown in Fig. 4. Although the intensity of the white line peak was slightly decreased after the reaction, the peak position did not change. This indicates that the 4d state, i.e., the oxidation state of the Pd species in the catalyst, did not markedly change after the reaction. That is, Pd(II) species are still present as the predominant Pd species. A slight decrease in the intensity should be caused by the presence of the Pd clusters as minor species.

From these results, the catalyst structure after the Heck reaction is determined as follows. On Pd-SH-FSM and Pd-SH–SiO_2, the Pd(II) complexes coordinated to at least two sulfur ligands are the main Pd species, together with the Pd clusters as the minor species. On ligandless Pd-FSM and previously reported catalysts (Pd-Y and Pd/C), most of the Pd species were reduced and aggregated to form metal particles (Pd-FSM and Pd-Y) or clusters (Pd/C).

3.4. Heterogeneity and recyclability of Pd-SH-FSM for the Heck reaction

Heterogeneity of Pd-SH-FSM for the Heck reaction of 4-bromoacetophenone and ethyl acrylate was examined by the "hot filtration test" [39]. After the reaction mixture was stirred for 10 min in the presence of 0.1 mol% Pd-SH-FSM (yield = 14%), the catalyst was filtered off at 373 K. With filtrate the reaction did not further proceed after 24 h, confirming the heterogeneous catalysis of Pd-SH-FSM. The Pd-

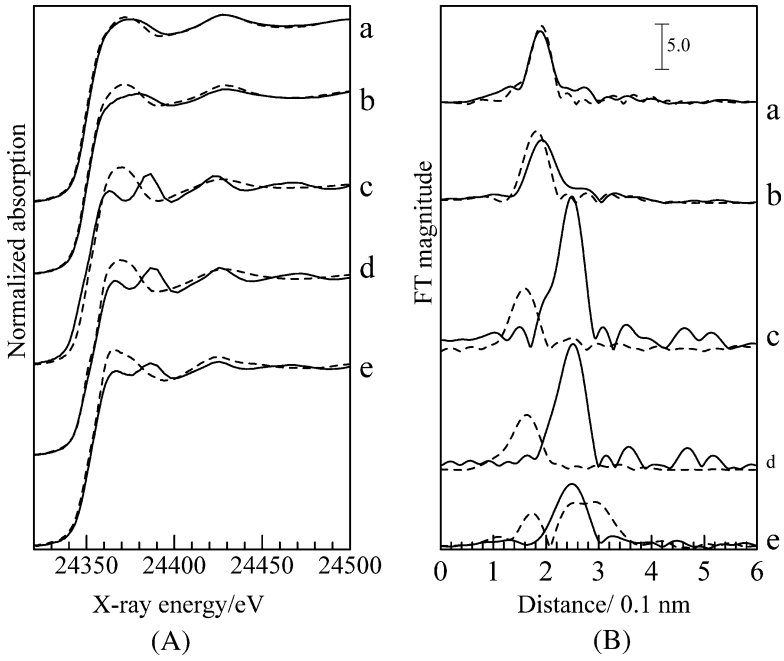

Fig. 9. (A) Pd *K*-edge XANES spectra and (B) Fourier transforms of k^3-weighted EXAFS spectra of the catalysts after the Heck reaction: (a) Pd-SH-FSM, (b) Pd-SH–SiO_2, (c) Pd-FSM, (d) Pd-Y, (e) Pd/C. Dotted lines denote the spectra for the fresh catalysts.

Table 5
Successive Heck reaction using recovered catalysts[a]

Cycles	Yield (Pd-SH-FSM) (%)	Yield (Pd-SH–SiO_2) (%)
	92	84
1st reuse	95	93
2nd reuse	97	88
3rd reuse	97	99
4th reuse	99	88
5th reuse	97	95

[a] Conditions: 4-bromoacetophenone (3.0 mmol), ethyl acrylate (4.5 mmol), KOAc (4.5 mmol), and the catalyst (1 mol%) were stirred in NMP (5 mL) at 403 K under N_2.

SH-FSM and Pd-SH–SiO_2 showed excellent recyclability for the Heck reaction (Table 5). The catalyst can be reused at least 5 times with no indication of the catalyst deactivation, which confirms the high stability of these catalysts.

We have also examined the activity of Pd-SH-FSM (1 mol%) for the Heck reaction of 4-bromoanisole, bromobenzene, and 4-chloroacetophenone with ethyl acrylate under the same conditions as in Table 1. Use of less reactive electron-rich aryl bromides, 4-bromoanisole and bromobenzene, resulted in moderate yields (58 and 62%, respectively). The reaction with 4-chloroacetophenone resulted in a low yield (18%).

3.5. Correlation of catalyst structure and activity for coupling reactions

Fig. 10 shows the time course of the Suzuki reaction of 4-bromoanisole and phenylboronic acid using the recovered catalyst after the Suzuki reaction (Table 1) well characterized in the above sections. Note that the kinetic experiment

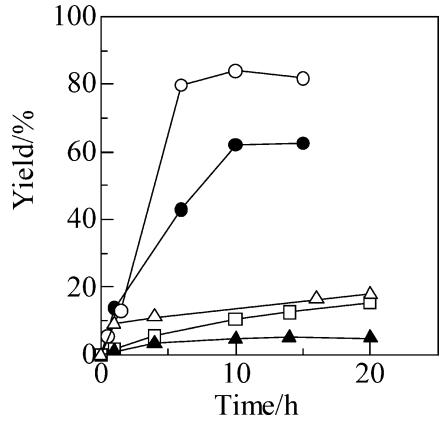

Fig. 10. Plot of GC yield versus time for the Suzuki reaction at 403 K with recycled catalysts after the Suzuki reaction in Table 1: (○) Pd-SH-FSM, (●) Pd-SH–SiO_2, (□) Pd-FSM, (▲) Pd-Y, (△) Pd/C. Conditions: 4-bromoanisole (25 mmol), phenylboronic acid (30 mmol), K_2CO_3 (37 mmol), DMF (50 mL), the catalyst amount (0.013 mol%).

in Fig. 10 was performed with low catalyst concentration (0.013 mol%) to evaluate differences in the reaction rates. Although the yield for the fresh catalyst in Table 1 was very close to each other, clear differences in the rate were observed under this condition. By comparing the slope of the curve, the structure–activity relationship of the reused catalysts can be discussed as follows. The reaction rate and the yield were considerably low with the reused Pd-FSM, Pd/C, and Pd-Y catalysts, in which most of the Pd species were changed to Pd metal particles during the first catalytic run. Higher reaction rates were observed for the reused Pd-SH-FSM and Pd-SH–SiO_2 catalysts, in which Pd species are stabilized by polydentate sulfur ligands. These results re-

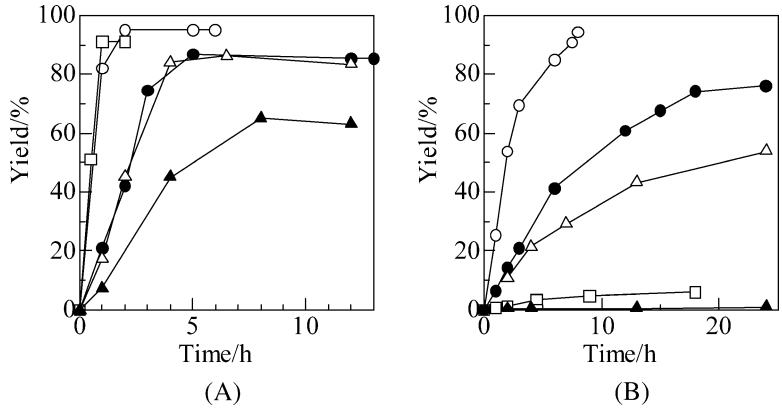

Fig. 11. Plot of GC yield versus time for the Heck reaction at 403 K with (A) fresh or (B) recycled catalysts: (○) Pd-SH-FSM and (●) Pd-SH–SiO_2 after the fifth cycle in Table 5; (□) Pd-FSM, (▲) Pd-Y and (△) Pd/C after the first cycle in Table 1. Conditions: 4-bromoacetophenone (50 mmol), ethyl acrylate (75 mmol), KOAc (75 mmol), NMP (50 mL) the catalyst amount (0.0013 mol%).

veal that highly dispersed Pd complexes have much higher activity for the Suzuki reaction than Pd metal particles. The lower activity of Pd-SH–SiO_2 than that of Pd-SH-FSM should be caused by the larger number of the Pd metal particles formed on Pd-SH–SiO_2 during the reaction, as noted above.

Fig. 11 shows the time course of the Heck reaction of 4-bromoacetophenone and ethyl acrylate with low catalyst concentration (0.0013 mol%). Fig. 11A is the kinetic result for the fresh Pd catalysts. Under this condition, clear differences in the activity were observed, and the reaction rate of the fresh catalysts increased in the order of Pd-SH-FSM = Pd-FSM > Pd-SH–SiO_2 = Pd/C > Pd-Y. For the fresh Pd-SH-FSM catalyst, turnover numbers (TON, moles of substrate/moles of Pd) as high as 73,000 and turnover frequencies of 36,000 h^{-1} were obtained, indicating the high activity and durability of the catalyst. By comparing the kinetic results of fresh (Fig. 11A) and reused (Fig. 11B) catalysts, it is clear that Pd-Y and Pd-FSM catalysts significantly deactivated after the Heck reaction (in Table 1, Pd = 1 mol%). The activity of Pd/C was also decreased after the first run, but the reused Pd/C showed higher activity than reused Pd-Y and Pd-FSM catalysts. Considering the characterization results, these results suggest that Pd metal clusters (2–10 nm) observed by TEM of Pd/C (Fig. 8c) have higher activity than larger metal particles on the latter catalysts. The kinetic experiments were also carried out using Pd-SH-FSM and Pd-SH–SiO_2 catalysts recycled after the fifth reuse in the Heck reaction (in Table 5, Pd = 1 mol%). Despite the severe recycling treatment, reused Pd-SH-FSM and Pd-SH–SiO_2 showed a higher reaction rate than Pd/C, Pd-Y, and Pd-FSM catalysts after the first use. It is significant to note that a complete conversion of 4-bromoacetophenone, 94% yield of the product, and a high TON (72,000) were attained with the Pd-SH-FSM even after the fifth reuse. Taking into account the structural information of the used catalysts, the above kinetic results reveal the following activity order of various Pd species for the Heck reaction: Pd complexes on the SH-functionalized silicas > metal clusters > larger metal particles. The SH groups anchored to the mesoporous silica supports are the most effective heterogeneous ligands for suppressing the aggregation of the dispersed Pd species, resulting in the most stable catalysis. The high reaction rate of the fresh Pd-FSM suggests that $Pd(OAc)_2$-like complexes on unmodified FSM have high activity. However, the characterization results and the reaction result in Fig. 11B revealed that most of the reactive complexes are converted to form inactive Pd metal particles in the absence of the SH ligands. This implies that mesoporous silica itself does not effectively prevent Pd metal aggregation. Because of the weak interaction between unmodified FSM and $Pd(OAc)_2$, "palladium dissolution and reprecipitation mechanism" [17,18,40] should be responsible for the high activity of the fresh Pd-FSM, where the solid supports is proposed to function as a reservoir for the leached Pd species as catalytic species. Our result clearly shows that, for this type of catalysis, the inorganic support does not prevent the metal agglomeration during reprecipitation, resulting in a significant deactivation.

From the above-noted discussions, it is clarified that the deactivation of the Pd(II) complexes in the Na-Y zeolite and in the unmodified mesoporous silica occurs via aggregation to inactive metallic particles. The PdO nanoclusters initially present in Pd/C are also in situ reduced and are converted to metallic Pd clusters, which have been shown to be less active for the Heck reaction than PdO nanoclusters. These results evidence that the formation of metallic Pd is a major cause of catalyst deactivation of previously reported solid catalysts for Heck and Suzuki reactions. Note that a moderate reaction rate of reused Pd/C for the Heck reaction (Fig. 11) suggests a moderate activity of Pd metal clusters. Among various supports tested in this study, the silica-immobilized polydentate sulfur ligands are indispensable for preventing the Pd metal agglomeration during Heck and Suzuki reactions. The mesoporous support (FSM-16) was more advantageous than amorphous silica for both Heck and Suzuki reactions, indicating a cooperating effect off the mesopore and the sulfur ligands for the stabilization of

the active Pd complexes. It is widely believed that, during the catalytic cycle, the Pd(II) complexes initially present in the catalyst are reduced to Pd(0) species, and unsaturated Pd(0) complexes can interact strongly with each other under the reaction condition to from Pd clusters [2,8]. Recently, Narayanan and El-Sayed reported a detailed TEM study on the particle-size growth during the Suzuki reaction by PVP-palladium nanoparticles [27]. They proposed that the observed increase in the particle size during the reaction is attributed to the Ostwald ripening in which small nanoparticles dissolve to from larger particles, and suggested that OH groups in PVP suppress the particle growth due to the inhibition of the Ostwald ripening process. According to their proposal, combined with the results in this study, we propose that the immobilization of Pd to the polydentate sulfur ligands in the mesopore restrict the mobility of reactive forms of Pd(II) and Pd(0) complexes, and thus intermolecular interaction of unstable Pd intermediates and resulting Ostwald ripening process can be retarded. In addition, the sulfur ligands in nanometer-sized channels of FSM-16 may surround Pd clusters once formed and suppress further aggregation, whereas clusters on the outer surface of SH-SiO_2 may grow further.

4. Conclusion

The stability toward the formation of inactive Pd metal particles is the crucial factor for achieving a stable heterogeneous catalysis for Heck and Suzuki reactions. The structural stability of Pd species can be controlled by using the appropriate support. As for the conventional catalysts (Pd zeolite and Pd/C), the Pd(II) species highly dispersed in the Na-Y zeolite or on the activated carbon are aggregated to form less active metallic particles or clusters. In contrast, the silica-immobilized SH groups act as polydentate ligands to stabilize Pd(II) species during Heck and Suzuki reactions. The sulfur ligands in the size-restricted mesopore of FSM-16 was most effective for preventing the Pd metal aggregation, which results in high durability and recycling characteristic of the Pd-SH-FSM. This catalyst provides a clean and convenient alternative for Heck and Suzuki reactions because of its heterogeneous nature, high durability (high TON), simple reaction procedures, and recyclability without a marked loss of the catalytic activity.

Acknowledgment

The X-ray absorption experiments were performed under the approval of the Photon Factory Program Advisory Committee (Proposal No. 2003G-274).

References

[1] R.F. Heck, Org. React. (N.Y.) 27 (1982) 345.
[2] P. Beletskaya, A.V. Cheprakov, Chem. Rev. 100 (2000) 3009.
[3] N. Miyaura, T. Yanagi, A. Suzuki, Synth. Commun. 11 (1981) 513.
[4] N. Miyaura, A. Suzuki, Chem. Rev. 95 (1995) 2457.
[5] B.M. Bhanage, M. Arai, Catal. Rev. 43 (2001) 315.
[6] M. Terasawa, K. Kaneda, T. Imanaka, S. Teranishi, J. Organomet. Chem. 162 (1978) 403.
[7] C.-M. Anderson, K. Karabelas, A. Hallberg, J. Org. Chem. 50 (1985) 3891.
[8] P.-W. Wang, M.A. Fox, J. Org. Chem. 59 (1994) 5358.
[9] Y. Wang, H. Liu, J. Mol. Catal. 45 (1988) 127.
[10] J. Kiviaho, T. Hanaoka, Y. Kubota, Y. Sugi, J. Mol. Catal. 101 (1995) 25.
[11] D.J. Macquarrie, S.E. Fairfield, J. Mater. Chem. 7 (1997) 2201.
[12] M.-Z. Cai, C.-S. Song, X. Huang, J. Chem. Soc., Perkins Trans. 1 (1997) 2273.
[13] M. Lagasi, P. Moggi, J. Mol. Catal. 182–183 (2002) 61.
[14] C.P. Mehnert, D.W. Weaver, J.Y. Ying, J. Am. Chem. Soc. 120 (1998) 12289.
[15] L. Djakovitch, K. Köhler, J. Am. Chem. Soc. 123 (2001) 5990.
[16] M. Dams, L. Drijkoningen, B. Pauwels, G. Van Tendeloo, D.E. De Vos, P.A. Jacobs, J. Catal. 209 (2002) 225.
[17] F. Zhao, B.M. Bhanage, M. Shirai, M. Arai, Chem. Eur. J. 5 (2000) 843.
[18] K. Köhler, R.G. Heidenreich, J.G.E. Krauter, J. Piestsch, Chem. Eur. J. 8 (2002) 622.
[19] K. Mori, K. Yamaguchi, T. Hara, T. Mizugaki, K. Ebitani, K. Kaneda, J. Am. Chem. Soc. 124 (2002) 11572.
[20] B.M. Choudary, S. Mandhi, N.S. Chowdari, L.M. Kantam, B. Sreedhar, J. Am. Chem. Soc. 124 (2002) 14127.
[21] E. Paetzold, G. Oehme, H. Fuhrmann, M.-M. Pohl, H. Kosslick, Micropor. Mesopor. Mater. 44–45 (2001) 517.
[22] E.B. Mubofu, J.H. Clark, D.J. Macquarrie, Green Chem. 3 (2001) 23.
[23] R.B. Bedford, C.S.J. Cazin, M.B. Hursthouse, M.E. Light, K.J. Pike, S. Wimperis, J. Organomet. Chem. 633 (2001) 173.
[24] C. Baleizao, A. Corma, H. Garcia, A. Leyva, Chem. Commun. (2003) 606.
[25] K. Shimizu, T. Kan-no, T. Kodama, H. Hagiwara, Y. Kitayama, Tetrahedron Lett. 43 (2002) 5653.
[26] M.T. Reetz, E. Westermann, Angew. Chem. Int. Ed. 39 (2000) 165.
[27] R. Narayanan, M.A. El-Sayed, J. Am. Chem. Soc. 125 (2003) 8340.
[28] Y. Li, X.M. Hong, D.M. Collard, M.A. El-Sayed, Org. Lett. 2 (2000) 2385.
[29] X. Feng, G.E. Fryxell, L.-Q. Wang, A.Y. Kim, J. Liu, K. Kemner, Science 276 (1997) 923.
[30] S. Chen, K. Kimura, Langmuir 15 (1999) 1075.
[31] S. Chen, K. Kimura, J. Phys. Chem. 105 (2001) 5397.
[32] S. Inagaki, Y. Fukushima, K. Kuroda, J. Chem. Soc., Chem. Commun. (1993) 680.
[33] K. Nishi, K. Shimizu, M. Takamatsu, H. Yoshida, A. Satsuma, T. Tanaka, S. Yoshida, T. Hattori, J. Phys. Chem. B 102 (1998) 10190.
[34] T.A. Stephenson, S.M. Morehouse, A.R. Powell, J.P. Heffer, G. Wilkinson, J. Chem. Soc. (1965) 3632.
[35] J. Hanawalt, H. Rinn, L. Frevel, Anal. Chem. 10 (1938) 457.
[36] C. Sugiura, M. Kitamura, S. Muramatsu, J. Chem. Phys. 85 (1986) 5269.
[37] Z. Zhang, W.M.H. Sachtler, H. Chen, Zeolite 10 (1990) 784.
[38] J.S. Bradley, in: G. Schmid (Ed.), Clusters and Colloids, VHC, Weinheim, 1994, p. 459.
[39] R.A. Sheldon, M. Wallau, I.W.C.E. Arends, U. Schuchardt, Acc. Chem. Res. 31 (1998) 485.
[40] S.S. Prockl, W. Kleist, M.A. Gruber, K. Köhler, Angew. Chem. Int. Ed. 43 (2004) 1881.